Dynamic modelling of a single-axis belt-drive system

Klaus Sollmann

Volkswagen Group, Commercial Vehicles Section,
Sedanstrasse 21, 30161 Hannover, Germany
E-mail: klaus_sollmann@yahoo.de

Musa Jouaneh*

Department of Mechanical, Industrial and Systems Engineering,
University of Rhode Island, Kingston, RI 02881, USA
E-mail: jouaneh@egr.uri.edu
*Corresponding author

Abstract: Belt-driven positioning stages are widely used in industrial positioning applications and offer a low cost alternative to lead or ball screw stages. Due to the elasticity of the transmission element and friction effects, a dynamic model of these stages is needed to accurately simulate their response. This paper addresses the development of a dynamic model of a single-axis belt-driven linear motion positioning stage actuated by a geared DC motor. The model represents the effect of the mass of the cart and the inertia of the pulleys, the stiffness of the belt, the non-linear friction in the pulleys and cart motion, and the dynamics of the motor. Experimental and simulation work is performed to compare the performance of the real system with the non-linear model, and the results show that the developed model can accurately represent the dynamics of the belt-driven stage.

Keywords: dynamic modelling; belt-drive; positioning-stage.

Reference to this paper should be made as follows: Sollmann, K. and Jouaneh, M. (2011) 'Dynamic modelling of a single-axis belt-drive system', *Int. J. Modelling, Identification and Control*, Vol. 12, No. 4, pp.386–394.

Biographical notes: Klaus Sollmann received his MS in Mechanical Engineering in summer 2007 from the University of Rhode Island, Kingston, RI, USA. In addition he received his Diploma Engineer degree from The Technical University of Braunschweig, Braunschweig, Germany in summer 2008. Currently, he is working as an Engineer in the Graduate Programme of the Volkswagen Group in the Commercial Vehicles section, Hannover, Germany. His research interests include integrated production systems, vehicle final assembly, production maintenance, mechatronics and manufacturing systems.

Musa Jouaneh received his BS in Mechanical Engineering in 1984 from the University of Louisiana at Lafayette, LA, USA and his Master and Doctorate in Mechanical Engineering from the University of California at Berkeley, CA, USA in 1986 and 1989 respectively. He has been working in the Department of Mechanical Engineering at the University of Rhode Island, RI, USA since 1990 and currently Professor and Director of the Mechatronics Laboratory. His research interests include mechatronics and robotics with particular interest in motion control systems. He has served as a consultant to many companies in the Northeast and has received two College of Engineering Faculty Excellence Awards and the URI Foundation Teaching Excellence Award. He is the author or co-author of over 60 publications including two US patents. He is a member of ASME and is a senior member of IEEE.

1 Introduction

Part positioning and manipulation is an important task in industrial applications. Many positioning devices are built using elastic transmission elements such as timing belts. Belt-driven positioning stages offer a low cost alternative to lead or ball screw stages since less precision parts are needed to transmit the rotational motion of the motors into a linear motion of the stage. Pulleys and timing belts are also comparably cheap machine elements, which are available in a variety of standard sizes. Furthermore, belt drives are known to be insensitive with regards to wheel alignment, which lowers costs for production and they are also comparably quiet power transmission systems (Haus, 1996).

The use of elastic transmission elements also causes the biggest disadvantage of belt-driven stages, which is uncertainty in end-effecter or stage position. For many applications, the stage position, for practical as well as economical reasons, is not available as a feedback signal for

controlling the system. This means that even if an accurate tracking of the angular position of the motor that drives the belt system was achieved, the end-effecter position may still deviate from the desired path due to stretching of the belt especially in situations such as fast acceleration and deceleration. Another effect making an accurate end-effecter control difficult is the presence of non-linear friction in the system. For these reasons, it is very helpful to develop dynamic models that can accurately reflect the behaviour of these stages. These models can be used to test and simulate effective control strategies for these stages.

A survey of the literature dealing with modelling and control of belt-driven positioning stages has been carried out. Li and Rehani (1996) have developed a rigid-body model of a belt-driven positioning table. The model was used in a tracking controller to compensate for table inertia and friction. Reference (Hace et al., 2005) includes a two-mass model of a single-axis belt drive system with non-linear friction applied at the actuator and at the load. Several authors discuss different control methods to control belt-driven stages. These methods include fuzzy-logic (Kulkarni and El-Sharkawi, 2001), sliding mode methods combined with Lyapunov design (Hace et al., 2001), and feed-forward compensators (Jayawardene et al., 2003; Li and Rehani, 1995).

This paper addresses the development of a dynamic model of a single-axis belt-driven linear motion positioning stage. The remainder of this paper is organised as follows. In Section 2, a linear dynamic model of the stage is developed. Section 3 compares the linear model results with experimental data. In Section 4, a non-linear model of friction is added to the dynamic model to improve its accuracy and experimental and simulation results are presented to compare the performance of the real system with the non-linear model. The concluding remarks are presented in Section 5.

2 Dynamic model

2.1 Equations of motion

A schematic of the single-axis belt drive system is shown in Figure 1. The cart, represented by the mass M, is driven on a linear bearing guide system, using a timing belt that wraps around two pulleys placed at either end of the linear guide. The left pulley is driven by a geared DC motor.

Figure 1 Schematic of a single-axis belt-drive system

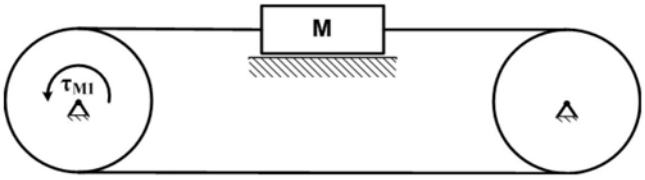

To develop the equations of motion describing the dynamic behaviour of such a system, the timing belt was assumed to have the behaviour of linear springs with a stiffness k_i; i = 1, 2, 3 as shown in Figure 2, also linear friction was initially assumed. The forces of the timing belt onto the cart as well as on the pulleys are of the form $F_{tb} = k \cdot \Delta l$, where Δl is the linear deformation of the spring and k is the spring constant; the friction force acting on the cart is of the form $F_{fr} = b \cdot v_{rel}$, where b is the linear motion viscous friction coefficient and v_{rel} is the velocity of the cart; and the friction torques acting on the pulleys are of the form $\tau_{fr} = B \cdot \omega_{rel}$, where B is the angular motion viscous friction coefficient and ω_{rel} is the angular velocity of the timing pulley.

Figure 2 Lumped parameter model of a single-axis belt drive system

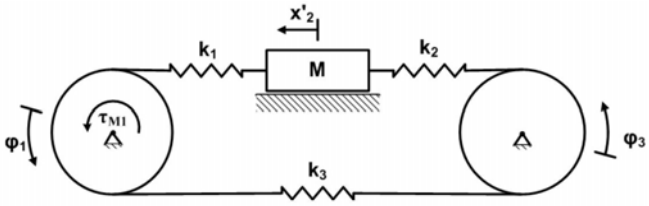

Through the application of Newton's laws of motion, it is straightforward to derive the following system of equations of motion that describe the dynamic behaviour of the system.

$$\ddot{\varphi}_1 = -(\varphi_1 r - x'_2) r k_1 \frac{1}{J_1} + (\varphi_3 - \varphi_1) r^2 k_3 \frac{1}{J_1} - \frac{B_1}{J_1}\dot{\varphi}_1 + \frac{\tau_M}{J_1} \quad (1)$$

$$\ddot{x}'_2 = (\varphi_1 r - x'_2)\frac{k_1}{M} - (x'_2 - \varphi_3 r)\frac{k_2}{M} - \frac{b}{M}\dot{x}'_2 \quad (2)$$

$$\ddot{\varphi}_3 = (x'_2 - \varphi_3 r) r k_2 \frac{1}{J_2} - (\varphi_3 - \varphi_1) r^2 k_3 \frac{1}{J_2} - \frac{B_2}{J_2}\dot{\varphi}_3 \quad (3)$$

where φ_1, φ_3 and x_2' are rotational and linear coordinates as shown in Figure 2, J_i (i = 1, 2) is the inertia of the pulleys, M is the mass of the cart, b, B_i (i = 1, 2) are friction coefficients, r is the radius of the pulleys, and τ_M is the motor torque applied, which is given by:

$$\tau_M = \frac{K_t}{R} V_{in} - \frac{K_t K_e}{R}\dot{\varphi}_1 \quad (4)$$

where V_{in} is the input voltage given to the permanent magnet brush type DC motor and therefore, the input signal to the one-axis belt drive system. K_t, K_e and R are the torque constant, the back-EMF constant and the resistance of the motor respectively. To simulate the system in Simulink, the model is transferred into state space form as shown in equation (5).

$$\begin{aligned} \dot{x} &= Ax + bu \\ y &= cx + du \end{aligned} \quad (5)$$

where A is the system matrix, b the input vector, c the output vector and d the feed through coefficient. By defining the state variables as:

$$\begin{aligned} x_1 &= \varphi_1 \qquad x_2 = \dot{\varphi}_1 \\ x_3 &= x'_2 \qquad x_4 = \dot{x}'_2 \\ x_5 &= \varphi_3 \qquad x_6 = \dot{\varphi}_3 \end{aligned} \tag{6}$$

We get the following expressions for the matrices:

$$A = \begin{bmatrix} 0 & 1 & 0 & 0 & 0 & 0 \\ -\frac{(k_1+k_3)r^2}{J_1} & -\frac{B_1}{J_1}-\frac{K_t K_e}{RJ_1} & k_1\frac{r^2}{J_1} & 0 & k_3\frac{r^2}{J_1} & 0 \\ 0 & 0 & 0 & 1 & 0 & 0 \\ \frac{k_1}{M} & 0 & -\frac{k_1+k_2}{M} & \frac{b}{M} & \frac{k_2}{M} & 0 \\ 0 & 0 & 0 & 0 & 0 & 1 \\ k_3\frac{r^2}{J_2} & 0 & k_2\frac{r^2}{J_2} & 0 & -\frac{(k_2+k_3)r^2}{J_2} & -\frac{B_2}{J_2} \end{bmatrix} \tag{7}$$

$$b = \begin{bmatrix} 0 \\ \frac{K_t}{RJ_1} \\ 0 \\ 0 \\ 0 \\ 0 \end{bmatrix} \tag{8}$$

$$c = \begin{bmatrix} 1 & 0 & 0 & 0 & 0 & 0 \end{bmatrix} \tag{9}$$

$$d = 0 \tag{10}$$

2.2 Experimental system

In this belt-driven stage, the timing belt is of the MXL series with 2.03 mm (0.080 inches) pitch, and a width of 9.53 mm (0.375 inches). The centre distance between the two pulleys is 787 mm and the overall length of the stage is 863 mm. The timing pulley has 60 grooves and a pitch diameter of 38.8 mm (1.528 inches). The motor that drives one of the pulleys is a Pitman Geared Motor (gear ratio is 5.9:1) with an optical encoder, Model GM9236C534-R2. The motor is rated at 30.3 volts and has a no load speed of 800 rpm. Angular position feedback information is obtained from the encoder, which has 512 lines per revolution and operates in quadrature mode. A PWM Servo Amplifiers, Model 12A8 from Advanced Motion Controls, amplifies the voltage signal that is sent to the DC motor from the D/A converter on the PC that controls this setup.

2.3 Determination of parameters

In order to accurately reflect the dynamic behaviour of the system, the parameters of friction, inertia and mass as well as stiffness have to be determined. Some of these parameters are not easy to determine, and iteration based on actual testing is used.

2.3.1 Stiffness

The stiffness of the belt sections were assumed to be of the form

$$k = \frac{AE}{l} \tag{11}$$

where A is the cross-section of the belt, E is the E-modulus, and l the length of the belt section. The belt cross section approximately consists of 2/3 neoprene ($E = 6 \times 10^6$ N/m^2) and 1/3 fibreglass ($E = 50 \times 10^9$ N/m^2) that can be treated as two springs in parallel. The modulus E of the belt was therefore initially estimated by adding 2/3*E_neoprene and 1/3*E_fibreglass. Since a timing belt consists of teeth and belt regions without teeth, the cross-section cannot be chosen trivially. However, if the regions with and without teeth are being considered as a serial connection of two springs as shown in Figure 3, then it can be seen that a good assumption is that the cross-section can be chosen to be that of the belt section region without teeth. This is because the equation for the effective stiffness of serial springs is:

$$k_{eff} = \frac{k_t k_{nt}}{k_t + k_{nt}} \tag{12}$$

Therefore, since $A_t >> A_{nt}$ and also $K_t >> K_{nt}$ this leads to the transformation of equation (12) to equation (13) below.

$$k_{eff} \approx k_{nt} = \frac{A_{nt} E}{l} \tag{13}$$

Note that in this system $l_1 = l_2 = 0.349$ m, and $l_3 = 0.787$ m.

Figure 3 Spring model of timing belt

2.3.2 Inertia and mass

For the derivation of the dynamic model the mass of the belt is assumed to be negligible compared to the inertia of the pulleys as well as to the mass of the cart. Thus, we are assuming that the mass of the cart and the inertia of the pulleys and not the mass of the belt are affecting the dynamic behaviour of the system. While the mass of the cart can be easily and precisely determined by disassembling and weighing it, the inertia of the pulleys could only be approximately determined. The approximation is based on the calculations obtained from a CAD model of the pulley, which has slight uncertainties since the exact composition of the aluminium alloy from which the pulley is made is not known, and the CAD model does not have all the geometric details of the real part.

2.3.3 Friction

Initially, the friction in the system was assumed to be caused by viscous effects. The value of the viscous friction coefficient b for the cart (B for the friction torques of the pulleys) is affected by different effects, the configuration of the surfaces rubbing against each other is one example for those effects, and the lubrication of the ball bearings of the

pulleys is another. Since values for the friction coefficients for this system were not available, experimental values for similar elements as used in the system, which were previously determined by one of the authors, where used as initial values for the dynamic model.

3 Modelling results

To verify the dynamic model as well as the assumptions made regarding the three stiffness coefficients, inertia and friction, the dynamic model was simulated in Simulink and compared to experimental data gained from the real system. Open loop tests were performed on the real system as well as open loop simulations with the previously obtained model. The test input signal is a 0.25 seconds long impulse of different voltages (5 V and 10 V). The equivalent motor linear position (converted into meters by multiplying the angular position by the pulley radius) and the equivalent motor linear velocity were recorded.

Table 1 Initial parameters for linear friction model

	Variable	*Value*
Radius	R	0.0194m
Belt area	A	5.5626×10^{-6} m^2
Belt modulus	E	16.67×10^{9} N/m^2
Stiffness	k_1	2.6552×10^{5} N/m
	k_2	2.6552×10^{5} N/m
	k_3	11.777×10^{4} N/m
Friction	B	0.0042 Nm s
	b	40.6518 (N s)/m
Inertia and mass	J	7×10^{-5} kg m^2
	M	0.362 kg
Motor constants	K_t	23×10^{-3} (N m)/A
	K_e	23×10^{-3} V/(rad s)
	R	0.71 Ω

In the real system, the data was recorded by timed data collection software programmed in Visual Basic that utilised the encoder measurements of the motor. For the dynamic system the A-, b-, and c-matrices of the state space model where computed with the parameters listed in Table 1.

The experimental and simulation plots are shown in Figure 4 and Figure 5. In those plots, it can be seen that the response of the simulated system does not match the experimental system very well. While the shape of the dynamic response is similar, the final steady state value of the simulated system is less than what was observed in the real system. Therefore, the values of the initial parameters will be changed to see what effect they have on the system response. In performing this, one parameter will be changed at a time while keeping the other two parameters constant. Therefore, plots were produced in which one of the parameters was doubled as well as halved, and the other parameters were left unchanged. This was done for each one of the three parameters. Those plots are shown in Figure 6–Figure 13. It can be seen from those plots, that friction has by far the biggest influence regarding the magnitude of the response. Inertia and stiffness have minor effects on the dynamics of the system. Figure 6–Figure 9 shows that changing the stiffness does not appreciably change the position response. Only the oscillation in the velocity profile changes marginally when the stiffness was changed by a factor of two. The inertia of the system determines the speed of the response, and Figure 10 and Figure 11 show as expected a slower response for higher inertia. However, the final position is the same, since a higher inertia also leads to a slower deceleration after shutting off the motor. Figure 12 and Figure 13 show the effect of changing the friction parameter value.

Figure 4 Motor position open loop response

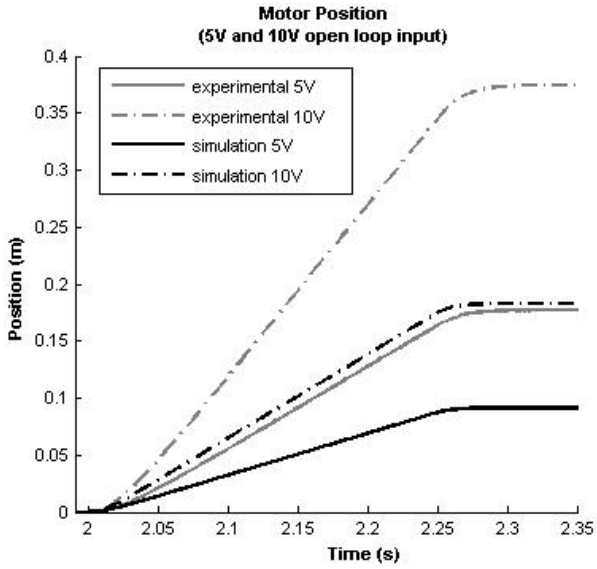

Figure 5 Motor velocity open loop response

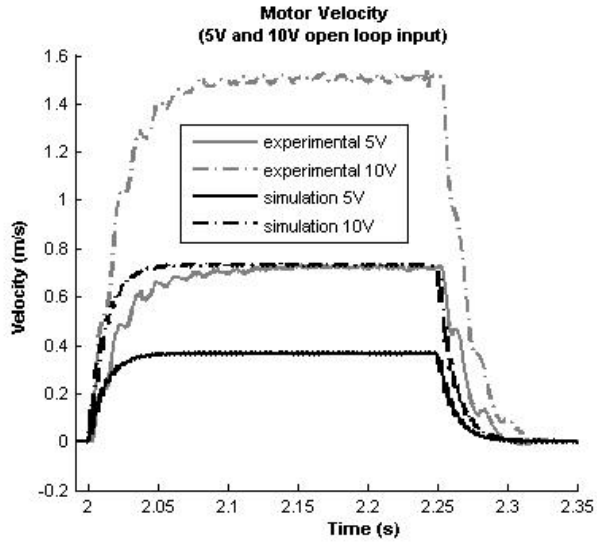

The next step was to find the correct values for each of the parameters in order to match the simulation response with the response of the real system. Due to the presence of non-linear friction, which was not accounted for in the initial derivation of the dynamic model, it is not possible to find just one set of parameters that fit the response of the real system for different input values. For example, if parameters were found to have a good match at 5 V, they will not work as well when the input is 10 V. As an illustration of this, Figure 14 and Figure 15 show the response of the simulated and real system for a set of parameters that fit the 5 V input well. The parameters for this case are listed in Table 2. Note the poor match in this plot for the 10 V input voltage case.

Figure 6 Motor position open loop response with increase in stiffness value

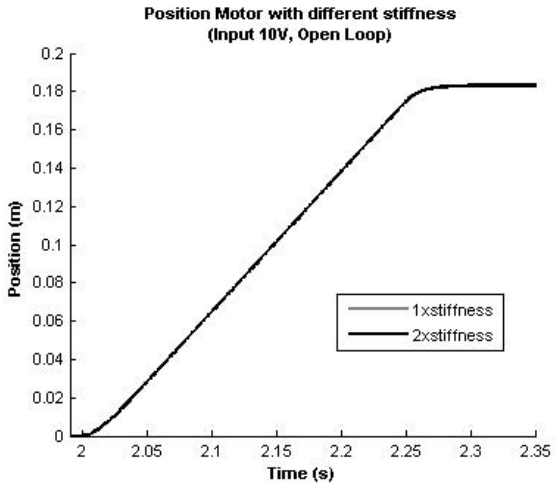

Figure 7 Motor position open loop response with decrease in stiffness value

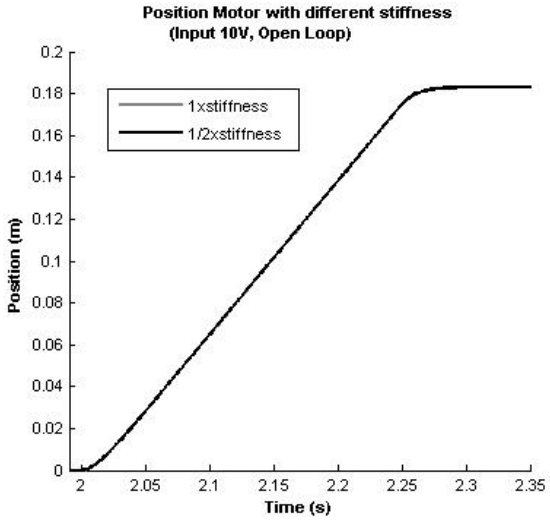

Figure 8 Motor velocity open loop response with increase in stiffness value

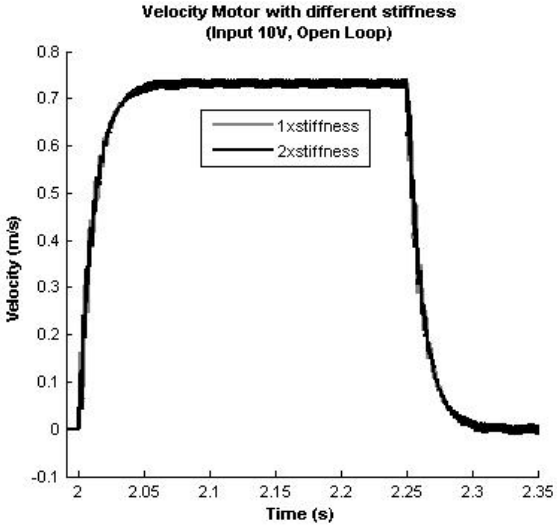

Figure 9 Motor velocity open loop response with decrease in stiffness value

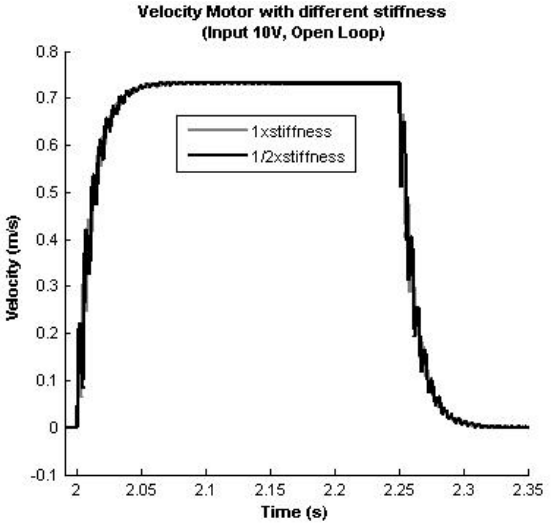

Figure 10 Motor position open loop response with different inertia parameters

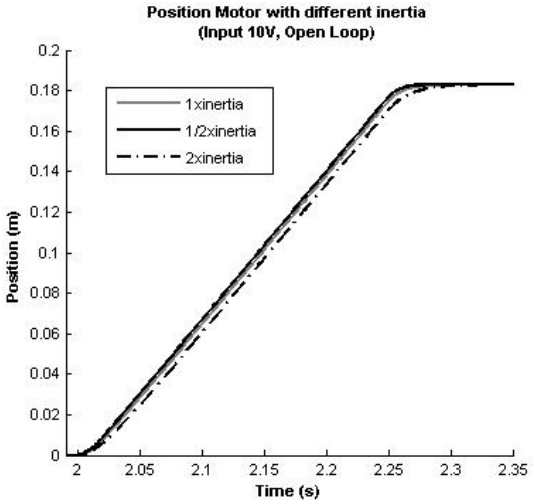

Figure 11 Motor velocity open loop response with different inertia parameters

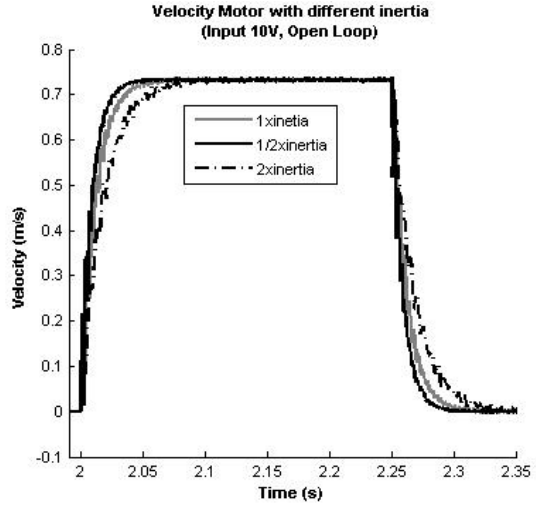

Figure 12 Motor position open loop response with different friction parameters

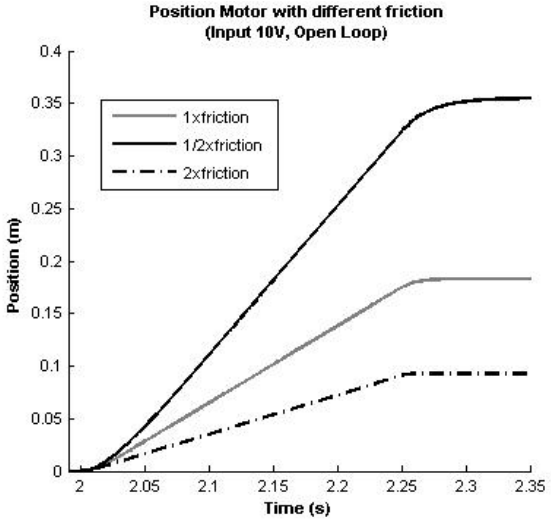

Figure 13 Motor velocity open loop response with different friction parameters

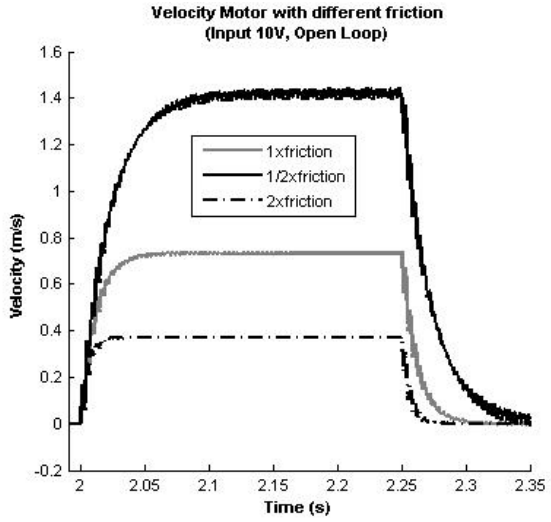

Figure 14 Motor position open loop response with parameters that were matched for 5 V input

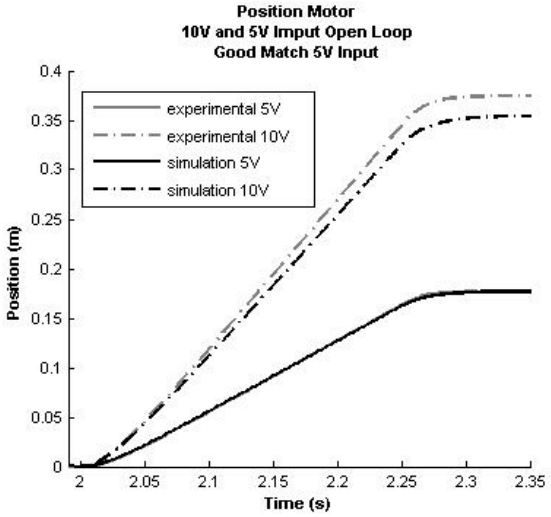

Figure 15 Motor velocity open loop response with parameters that were matched for 5 V input

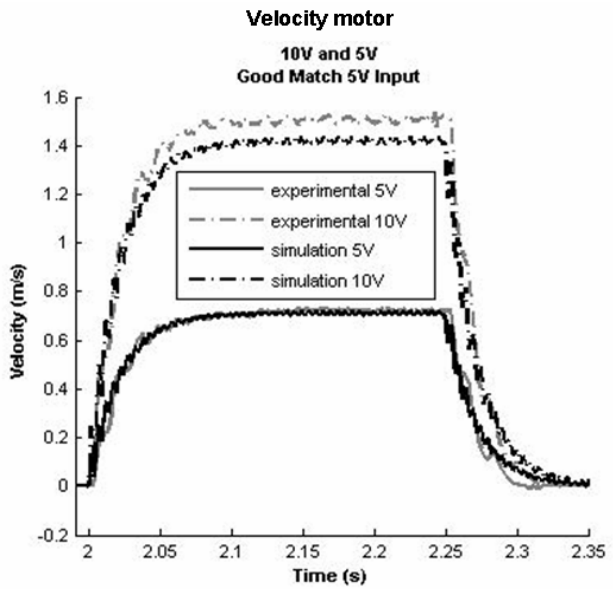

Table 2 Parameters for linear friction model matched for 5 V input

	Variable	*Value*
Radius	R	0.0194m
Belt area	A	5.5626×10^{-6} m^2
Belt modulus	E	8.335×10^{9} N/m^2
Stiffness	k_1	1.3276×10^{5} N/m
	k_2	1.3276×10^{5} N/m
	k_3	5.8885×10^{4} N/m
Friction	B	0.0021 Nm s
	b	20.3259 (N s)/m
Inertia and mass	J	6.3×10^{-5} kg m^2
	M	0.362 kg
Motor constants	K_t	23×10^{-3} (N m)/A
	K_e	23×10^{-3} V/(rad s)
	R	0.71 Ω

4 Non-linear model of the one-axis system

As discussed before, the derived linear model can accurately reflect the response around one input voltage. In control applications however the input voltage is not necessarily well predictable and most certainly not constant, since in closed loop control the input voltage to the plant is error driven. Therefore, it is desirable to come up with a simulation model that is not limited to a small input range. Initially, the friction in the stage was assumed to be strictly viscous whose value is proportional to speed. This means that around zero velocity the friction force/torque is practically zero. However, this is not the case for the real system.

A commonly used model (Feemster et al., 1999) for non-linear friction is shown in equation (14) below. Armstrong-Helouvry (1993, 1994), and Grami and Bigras (2008) discuss various friction models.

$$F_f = b \cdot v + sign(v) \cdot F_c + sign(v) \cdot F_s \cdot e^{(-F_\tau \cdot v^2)} \tag{14}$$

The model consists of three terms describing three different friction related effects. The first term describes the viscous friction, which what was assumed so far. The second term accounts for the Coulomb friction, which is an offset value that is dependent on the direction of motion. This effect accounts for the fact that for velocities close to zero the friction force is not zero. The third and last term is called Stribeck effect. It is based on the observation that the friction drops a certain amount after motion has started. Ff, F_c and F_s in the equation are called the friction force, the Coulomb force and the static force respectively. F_τ is the Stribeck related positive parameter and b the viscous friction coefficient. The three effects as well as their combined effect are visualised in Figure 16.

Figure 16 Non-linear friction model including Stribeck effect

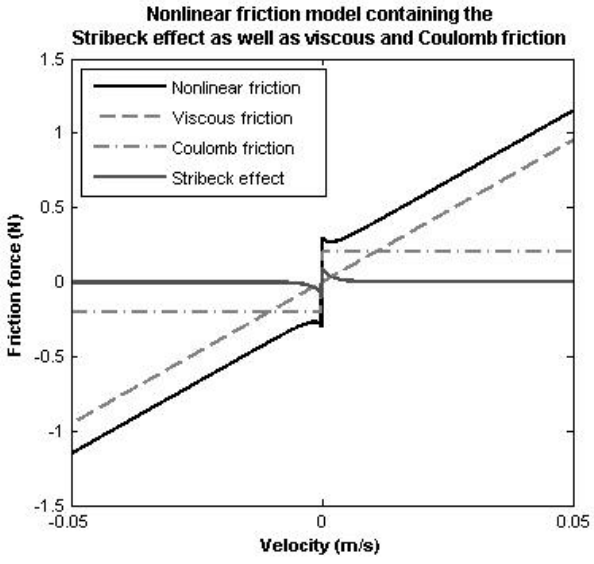

The Stribeck effect captures however only a minor effect of the friction behaviour and was neglected in our model. Thus, the friction model that we considered had only the viscous and the Coulomb friction, as shown in equation (15).

$$F_f = b \cdot v + sign(v) \cdot F_c \tag{15}$$

Similarly, a friction torque can be expressed by changing the forces in the above equation to torques, the linear velocity to angular velocity and by adjusting the parameters. Figure 17 shows the friction model described in equation (15).

In order to model the non-linear friction and simulate it in Simulink the strictly linear state space block cannot be used anymore to represent the now non-linear plant. To be able to account for the non-linearity, each equation from the set of equations of motion has to be represented as a block diagram on its own. Equations (16) through (18) show the set of equations of motion in this form utilising the elements of the state space vector to represent the displacement, velocity and acceleration of the original coordinates shown in equation (6).

Figure 17 Non-linear friction model with only viscous and Coulomb effects

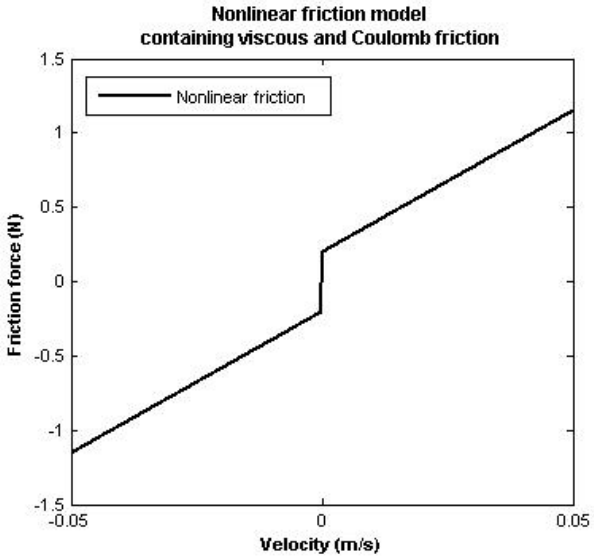

$$\dot{x}_2 = \frac{1}{J_1}\left(-\left(x_1 r - x_3\right) r k_1 + \left(x_5 - x_1\right) r^2 k_3 - \tau_{f_1} + \tau_M\right) \tag{16}$$

$$\dot{x}_4 = \frac{1}{M}\left(\left(x_1 r - x_3\right) k_1 - \left(x_3 - x_5 r\right) k_2 - F_f\right) \tag{17}$$

$$\dot{x}_6 = \frac{1}{J_2}\left(\left(x_3 - x_5 r\right) r k_2 - \left(x_5 - x_1\right) r^2 k_3 - \tau_{f_2}\right) \tag{18}$$

Figure 18 shows as an example, how equation (16) is transferred into a Simulink block diagram. The diagram takes the displacements x_1, x_3 and x_5 as well as the Voltage input to the motor V_{in} as an input and returns the velocity x_2 of the motor pulley. In the upper left hand corner of the block diagram it can be seen how the displacements x_1, x_3 and x_5 are used to calculate the spring torque which is applied to the motor pulley through the belt. This part of the block diagram represents the first two sets of parenthesis in

equation (16). In the lower part of the diagram, it is shown how the input Voltage V_{in} as well as the fed back velocity x_2 are used to calculate the motor torque τ_M according to equation (2). Finally, the embedded Matlab function in the upper half of the block diagram is used to compute the non-linear friction torque τ_{f_1}. This function takes the motor pulley velocity x_2, the values of the two constants B_1 and τ_c which are the viscous friction coefficient and the Coulomb torque respectively, as well as the sum of the spring and the motor torques (the computed torque acting on the pulley) as inputs and returns the friction torque τ_{f_1}. Table 3 shows the code that is being computed while executing that function. The function calculates first a temporary friction torque $\tau_{f_{1_{tmp}}}$. Friction torques and friction forces have the characteristic to only oppose a motion; however, they would not actually change the direction of the motion, since it is a passive force/torque. This is where the Coulomb friction model creates a problem if not implemented properly. The offset values of friction force/torque close to zero may actually change the direction of motion. This is what the if-loop in the function is preventing; it sets the actual friction torque to the computed torque if the friction torque is greater than the computed torque in a velocity band close to zero in order to cancel out the computed torque and to prevent a change in direction of motion. This friction torque is then being subtracted from the computed torque, which completes the bracket expression. The result of that subtraction is then divided by J_1, which according to equation (16) then gives the acceleration of the motor pulley. The acceleration is then integrated to obtain the velocity.

A similar block diagram is generated for each one of the non-linear equations of motion, with each having a function to account for the non-linear friction occurring in that equation. Those three block diagrams are then assembled to form the dynamic model. In this setup, the output velocity from each equation block diagram is integrated to obtain the position, which when added to the velocities completes the whole state vector. The position is also fed back as the input to the individual block diagrams of each axis. The final simulation model is shown in Figure 19. The motor gain seen in this block diagram is the amplifier gain, which is also present in the real system, which for the linear case is included as part of the input vector *b*.

With this non-linear model of the plant, it should now be possible to find one set of parameters including the Coulomb friction force/torques that makes it possible to match any arbitrary input value. The set of friction parameters that were found are given in Table 4. Figure 20 and Figure 21 show real and simulated plots of the stage position and velocity, respectively where the non-linear friction model was utilised in the simulation. It can be seen now that both the 5 V and the 10 V input experimental data can be matched well in contrast to what was obtained with the linear friction simulation (Figure 14 and Figure 15).

Table 3 Code for non-linear friction force/torque

```
function Tauf =
fcn(phidot,B1,Tauc_1,TauComputed)
        Tauf_tmp = B1*phidot + sign(phidot)*Tauc_1;
        if phidot> = –0.01 && phidot<=0.01 &&
abs(TauComputed)< = Tauc_1
                Tauf = TauComputed;
        else
                Tauf = Tauf_tmp;
        end
end
```

Figure 18 Block diagram of non-linear model of equation (17) in Simulink

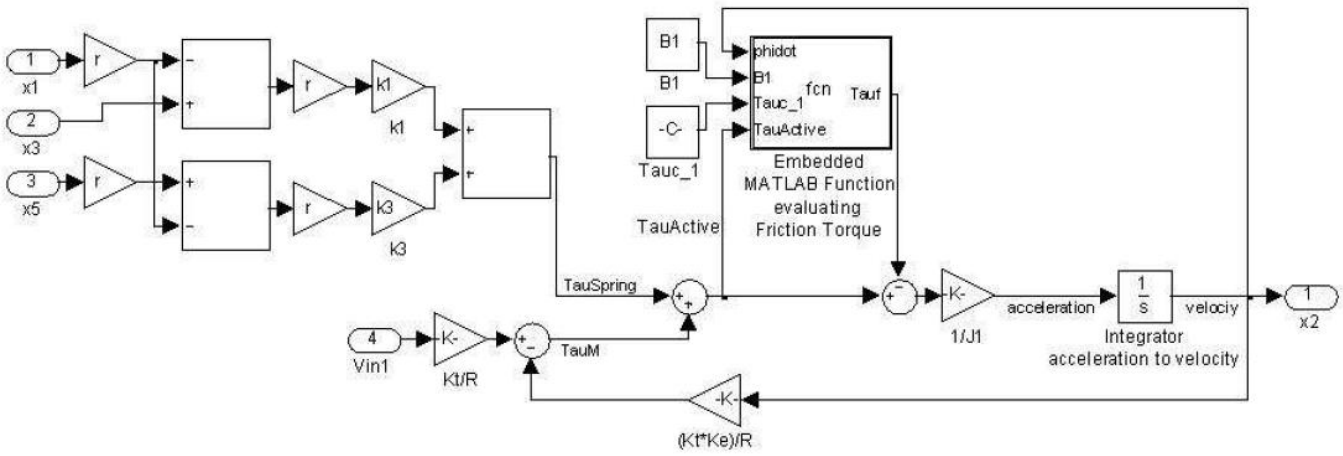

Figure 19 Simulation model in Simulink

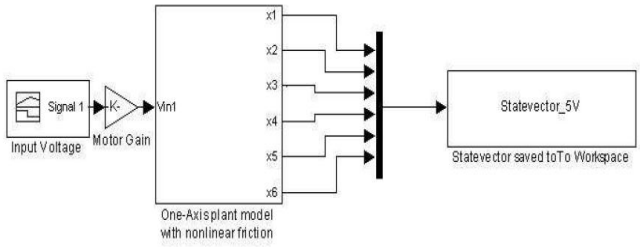

Table 4 Parameters for non-linear friction model

	Variable	*Value*
Viscous	B1	0.0016 Nm s
	B2	0.0016 Nm s
	B	19.0424 (N s)/m
Coulomb	τ_{c1}	0.0150 Nm
	τ_{c2}	0.0150 Nm
	F_c	0.2000 N

Figure 20 Experimental and non-linear model open loop position response

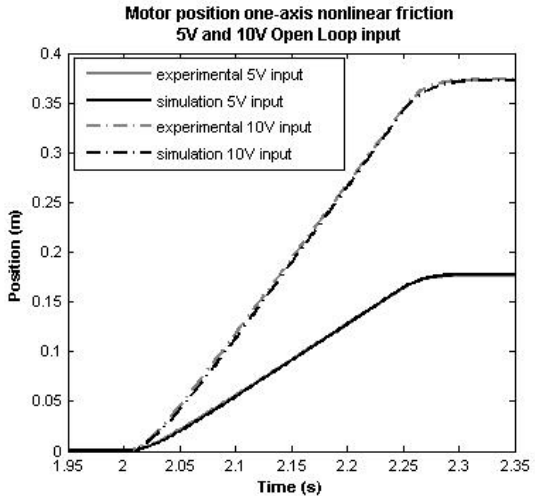

Figure 21 Experimental and non-linear model open loop velocity response

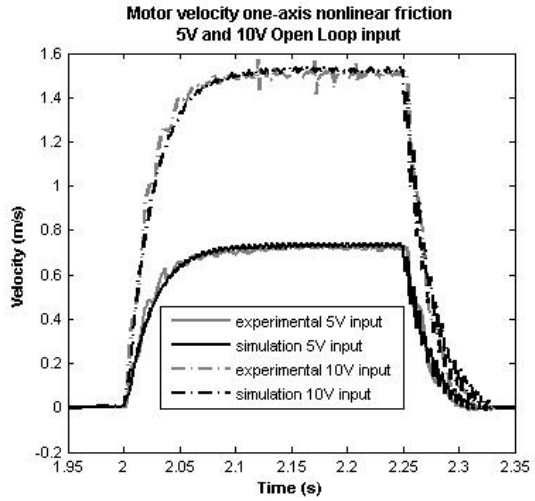

5 Conclusions

In this paper, a linear dynamic model representing the dynamic behaviour of the studied one-axis belt drive system was first derived. After parameters were determined, it was shown that this model can only match experimental results obtained from the real system for a small range of input values. Non-linear friction was found to be the major source of the non-linearities in this system, and a non-linear model reflecting the non-linear friction was added to the dynamic model. It was shown that with this non-linear model experimental data for multiple input voltages could be matched in simulation. The designed model can be used to design and simulate various controllers for controlling the motion of the stage.

References

Armstrong-Helouvry, B. (1993) 'Stick slip and control in low-speed motion', *IEEE Transactions on Automatic Control*, Vol. 38, No. 10, pp.1483–1496.

Armstrong-Helouvry, B., Dupont, P. and Canudas De Wit, C. (1994) 'Survey of models, analysis tools and compensation methods for the control of machines with friction', *Automatica*, Vol. 30, No. 7, pp.1083–1138.

Feemster, M., Vedagarbha, M., Dawson, M. and Haste, D. (1999) 'Adaptive control techniques for friction compensation', *Mechatronics*, Vol. 9. pp.125–145.

Grami, S. and Bigras, P. (2008) 'Identification of the GMS friction model based on a robust adaptive observer', *International Journal of Modelling, Identification and Control*, Vol. 5, No. 4, pp.297–304.

Hace, A., Jezernik, K. and Sabanovic, A. (2005) 'Improved design of VSS controller for a linear belt-driven servomechanism', *IEEE/ASME Transactions on Mechatronics*, Vol. 10, No. 4, pp.385–390.

Hace, A., Jezernik, K. and Terbuc, M. (2001) 'VSS motion control for a laser-cutting machine', *Control Engineering Practice*, Vol. 9, No. 1, pp.67–77.

Haus, R. (1996) 'Converting rotary motion to linear motion', *Power Conversion and Intelligent Motion*, Vol. 22, No. 11, pp.72–75.

Jayawardene, T., Nakamura, M. and Goto, S. (2003) 'Accurate control position of belt drives under acceleration and velocity constraints', *International Journal of Control, Automation, and Systems*, Vol. 1, No. 4, pp.474–483.

Kulkarni, A. and El-Sharkawi, M. (2001) 'Intelligent precision position control of elastic drive systems', *IEEE Transaction on Energy Conversion*, Vol. 16, No. 1, pp.26–31.

Li, W. and Rehani, M. (1995) 'Advanced tracking control of positioning tables', in *Proceedings of SPIE Int. Conference on Intelligent Manufacturing*, June, Vol. 2620, pp.786–791, Wuhan, China.

Li, W. and Rehani, M. (1996) 'Modeling and control of a belt-drive positioning table', in *Proceedings of the 1996 IEEE 22nd International Conference on Industrial Electronics, Control, and Instrumentation, IECON*, August, Vol. 3, pp.1984–1988, Taipei, Taiwan.